



Mccay, A. , Shipton, Z. K., Lunn, R. J. and Gale, J. F. (2019) Mini thief zones: Sub-centimeter sedimentary features enhance fracture connectivity in shales. *AAPG Bulletin*, 103(4), pp. 951-971.  
(doi:[10.1306/0918181610617114](https://doi.org/10.1306/0918181610617114))

There may be differences between this version and the published version. You are advised to consult the publisher's version if you wish to cite from it.

<http://eprints.gla.ac.uk/171718/>

Deposited on: 6 December 2018

Enlighten – Research publications by members of the University of  
Glasgow

<http://eprints.gla.ac.uk>

## Mini thief zones: Sub-centimeter sedimentary features enhance fracture connectivity in shales

Alistair T. McCay<sup>1\*</sup>, Zoe K. Shipton<sup>1</sup>, Rebecca J. Lunn<sup>1</sup>, and Julia F. Gale<sup>2</sup>

1. Engineering Geosciences and Geomechanics, Department of Civil and Environmental Engineering, University of Strathclyde, James Weir Building, Glasgow, G1 1XL.

2. The University of Texas at Austin, Bureau of Economic Geology, PO Box X, Austin, TX 78713-8924.

\*. Now at, [alistair.mccay@glasgow.ac.uk](mailto:alistair.mccay@glasgow.ac.uk), Systems, Power and Energy, School of Engineering, University of Glasgow, Glasgow, G12 8QQ.

### Acknowledgements

This work was funded by Nuclear Decommissioning Authority EPSRC CASE award GR/T11340/01. The authors would like to thank Dr Keith Ingham for introducing us to the field area and providing excellent base maps, and Dr. Simon Norris from the NDA for support and patience during the Ph.D.

### Abstract

This study examines the influences on fluid flow within a shale outcrop where the networks of two distinct palaeo-flow episodes have been recorded by calcite-filled veins and green alteration halos. Such direct visualisation of flow networks is relatively rare and provides valuable information of fluid flow behaviour between core and seismic scale.

Detailed field mapping, fracture data, and sedimentary logging were used over a 270m<sup>2</sup> area to characterise the palaeo-fluid flow networks in the shale. Distal remnants of turbidite flow deposits are present within the shale as very thin (1-10mm) fine grained sandstone bands. The shale is cut by a series of conjugate faults and an associated fracture network; all at a scale smaller than seismic detection thresholds. The flow episodes utilised fluid flow networks consisting of subgroups of both the fractures and the thin turbidites. The first fluid flow episode network was mainly comprised of thin turbidites and shear fractures, whereas the network of the second fluid flow episode was primarily small joints (opening mode fractures) connecting the turbidites.

The distribution of turbidite thicknesses follows a negative exponential trend; which reflects the distribution of thicker turbidites recorded in previous studies. Fracture density varies on either side of faults, and is highest in an area between closely spaced faults. Better predictions of hydraulic properties of sedimentary-structural networks for resource evaluation can be informed from such outcrop sub-seismic scale characterisation. These relationships between the sub-seismic features could be applied when populating discrete fracture networks models, for example, to investigate such sedimentary-structural flow networks in exploration settings.

### 1. Introduction

Shales, mudstones or mudrocks (shale differentiated by higher fissility) account for approximately two thirds of the sedimentary rock covering the Earth's surface (Aplin and Macquaker 1999). Many industries require a solid understanding of the hydraulic properties of shales, for instance as top seals for conventional oil and gas reservoirs or CO<sub>2</sub> storage targets (Gaus 2010); reservoirs for unconventional hydrocarbon production (Gale et al. 2014); geological disposal sites for radioactive waste disposal (Kim et al. 2011); geothermal resources (Wilmot-Noller and Daly 2014). However, there are issues with being able to capture their permeability properties at the appropriate scale and

then being able to upscale to whole reservoir perspective. Shales typically have low permeability (Dewhurst and Siggins 2006, Armitage et al. 2011, Aplin and MacQuaker 2011) and must be stimulated using hydraulic fracture treatments for hydrocarbon production. In order to enhance production it is advantageous if the hydraulic fractures connect the wellbore with higher permeability structures in the rock. Natural fractures, even if sealed, can be reactivated during treatments, and if open fracture networks are present, fluid flow will be strongly controlled by the linked natural and stimulated fracture network (Gale et al 2007). Shale units can also be interbedded with coarser material, such as siltstone or sandstone, due to depositional cycles such as turbidite flows (figure 2.13, Bouma et al. 1962). However the difficulty of making in-situ observations of the effects of thin, high-permeability beds (sometimes referred to as “thief zones” in thicker units) has hampered efforts to understand their effect on flow within a larger network.

Fracture networks in tight rocks may be beneficial because they can increase completion quality in shale gas and tight gas wells (e.g. Glaser et al. 2013), or may be detrimental by providing leakage pathways (Gaus 2010). Fault zones in sedimentary environments have been extensively studied for their flow properties (Lehner and Pilaar, 1997; Yielding et al., 1997; Dockrill and Shipton 2010; Davatzes and Aydin 2003; Eichhubl et al., 2005) due to the role of faults in compartmentalisation of reservoirs and hydrocarbon trapping. Faults can also provide conduits for along-fault flow as evidenced by diagenetic alteration surrounding fault related fractures e.g. mineralisation induced colour changes (Eichhubl et al. 2009), mineralisation within fractures ( Zhao et al. 2007, Kampman et al. 2012), modern springs (Fairley and Hinds 2004) and ancient CO<sub>2</sub> rich springs in the form of travertine mounds (Burnside et al. 2013).

Seismic techniques occasionally permit direct visualisation of fluid moving through faulted shales (i.e. seals) in the subsurface (Cartwright et al. 2007, Haney et al. 2005), but typically the structures controlling flow on the scale of the well are too small to be captured in reflection seismic data. On the other hand, cores from wellbores may only capture a small part of the permeability network and may not be representative of the larger scale. While many studies examine matrix permeability of core samples (e.g. Bolton et al. 2000, Aplin and Macquaker 2011), these are not representative of the bulk permeability of a fractured or faulted shale. Some studies have focussed on fault-related fractures, while others include the widely developed opening-mode fractures that occur in panels of rock away from faults (e.g. Lash and Engelder 2009, Gale et al. 2007, Evans 1994).

Outcrop analogue studies of fault and fracture systems in shale can be a useful scale bridge between core and seismic but are hampered due to the susceptibility of the rock to erosion leading to poor quality exposures. We investigated an exceptionally well-exposed shale unit hosting very thin (<1cm) sandy remnants of distal turbidite flows (Ingham 1978) and which is cut by sub-seismic scale faults. Distal regions of turbidite systems have previously been studied to understand their depositional environments (e.g. Crimes 1973), or the influence of turbidite sheet connectivity on hydrocarbon migration (Walker 1978). They are generally expected to form seals to hydrocarbon flow since any thin coarser grained layers lack vertical connectivity. We examine whether the sealing potential of shales in such distal turbidite regions is compromised by the presence of vertically connected subseismic fault and fracture networks in addition to the presence of rare injectites. Evidence is presented, collected from a distal portion of a turbidite system, of two separate fluid flow episodes identified by the presence of mineralisation and chemical alteration halos. A detailed study of the small scale sedimentary and structural features show that they interact, forming connected fluid flow networks through the mudstone. The results form the basis for a discussion about data collection strategies for aiding the detection and prediction of such networks in an applied setting.

## 2. Geological Setting

### 2.1 Field site location

The study area (figure 1), known as the Whitehouse Shore, is located in the southwest of Scotland, 3 km (2 miles) south of the town of Girvan. Interbedded, steeply dipping beds of sandstones and shales are exposed in the intertidal zone below a raised beach. The shale unit of interest is swept clear of debris with each tide, leaving the rock surface smooth and accessible for about 2.5 hours either side of low tide.

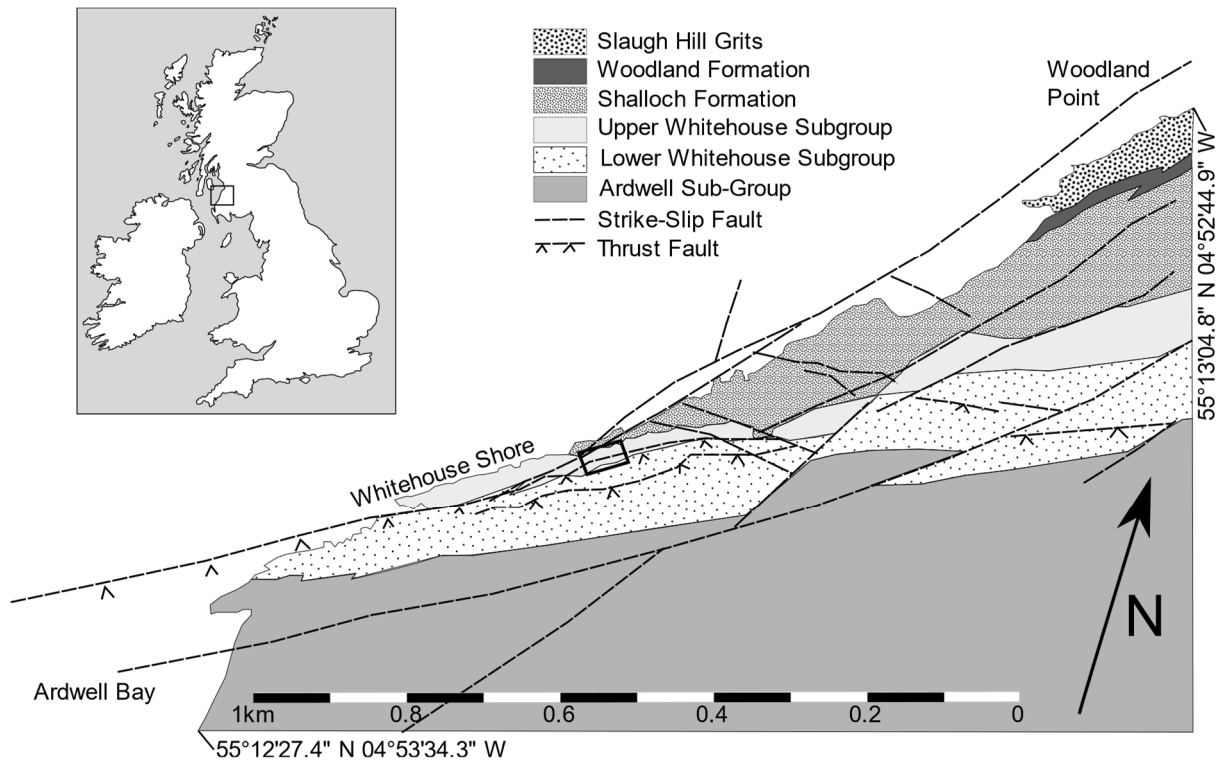


**Figure 1.** Geological map of the area surrounding Whitehouse Shore and the field site. Rocks are Ordovician and Silurian and young to the North East. Map from (Lawson and Weedon 1992). Field site is located at co-ordinates  $55^{\circ}12'49.47''\text{N } 004^{\circ}53'18.25''\text{W}$

The study area was chosen for two main reasons: 1) the unusually excellent exposure of mudrocks has undergone very low grade metamorphism, increasing resistance to erosion and therefore preserving the outcrop; 2) there is clear evidence of two distinct fluid flow episodes preserved in the rock. This site, the Whitehouse Shore, is a Site of Specific Scientific Interest (a UK classification of strict environmental and geological protection) and therefore no tools are permitted for sampling, all samples were from loose rock.

### 2.2 Sedimentary Setting

The Whitehouse Shore exposes Late Ordovician to Silurian sediments (figure 2) deposited within a submarine fan system that developed in a fore arc basin related to the closing of the Iapetus Ocean (Ince 1984). The Ballantrae Ophiolite, related to this closure, is located several miles to the south of the field site. Sedimentology suggests sourcing from a magmatic arc with palaeocurrent indicators showing sourcing from the North West (Hubert 1966).

At this field locality greywackes, sandstones, siltstones, mudstones, shales and thin limestones were deposited in waters over 400 m (1300 feet) deep in the Late Ordovician (Lawson and Weedon 1992). Significant variations in sediment thicknesses of the underlying Benan Conglomerate suggest that

the basin was bounded by active normal faults that controlled sedimentation on the fan (Ingham 1978). The Myoch Formation of the Upper Whitehouse subgroup is composed of predominantly green shale at its base overlain by red shale containing thin (often <1cm thick) sandstone bands. The Upper Whitehouse subgroup has been interpreted as deposited in a deep shelf and ocean floor setting distal to the submarine fan (Ingham 1978). This study focuses on the red shale member of the Myoch Formation, where the diagenetic features are most clear.

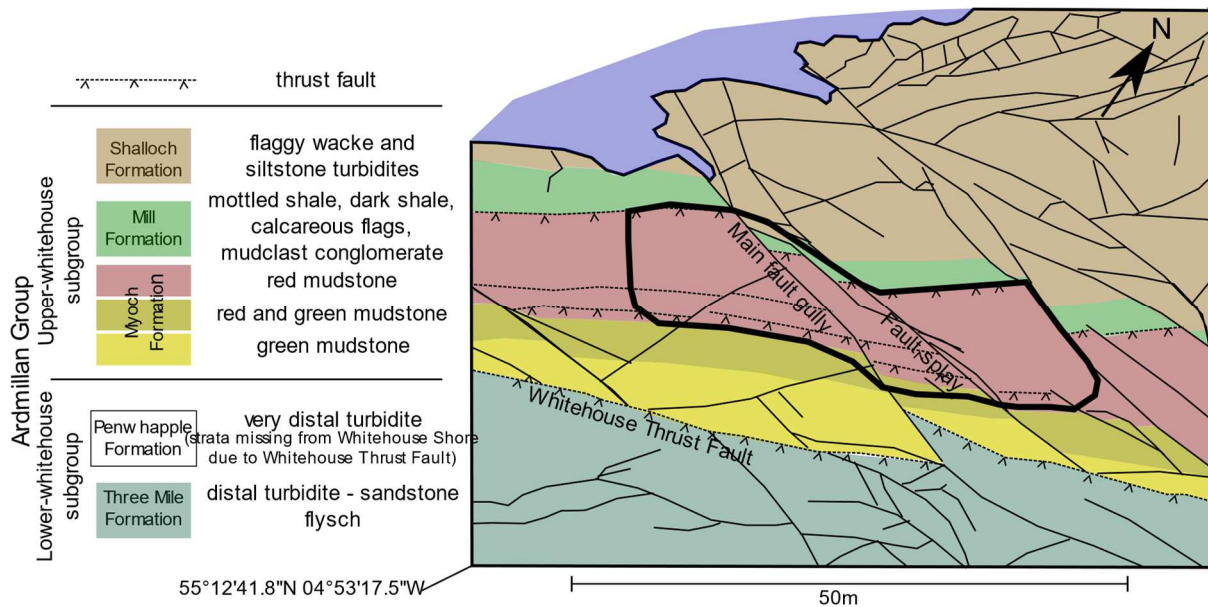


**Figure 2.** Geological map of the Whitehouse Shore (adapted from (Lawson and Weedon 1992)). The area highlighted by the thick black outline is the area of particularly good exposure used in this study which is mapped in detail on figure 9. Bedding dips 84-88° to the North-East and youngs in this direction. Earlier thrust faults are offset by later strike-slip faults. Photos a and b show particular interesting details of the fault core area. Photo a shows zone in footwall adjacent to fault core where sandstone bands (surrounded by green halo) are dragged into fault with strain being accommodated through shear fractures offsetting the thin sedimentary layer. Photo b shows area of fault core between two shear zones (shown by thick black lines), this area is highly fractured and pieces of fault core can be easily removed by hand whereas areas just outside shear zones are intact between fractures (e.g. those fractures shown in photo a). Red circle on map shows approximate location of photo a and b.

To characterise the shale, grain size and composition were estimated from point counting on SEM images. The grain size of the shale ranges from clay to rare grains of very fine sand (< 125µm to 63µm), although most of the grains are silt (< 63µm) or smaller with approximately 50% of the grains being part of the clay fraction. The mineral composition of the red shale is 10% quartz, 63% feldspar, with biotite, chlorite and metal oxides making up the remaining 27%. The thin sandstone bands within the red shale have steep dips of 84°-86° and have tightly clustered strikes of NE-SW (figure 3). The sandstone grain size ranges from 17µm (medium silt) to a maximum measured grain size of 148µm (medium sand). No grading of grain size was observed in any of the sandstone bands. Point counting gives a clay content of the sandstone bands as 20% and the composition of the clasts as 56% quartz, 12% feldspar, with the remaining 32% composed of biotite, chlorite and metal oxides. The partial replacement of some biotite grains with chlorite indicates that the shale has undergone very low grade metamorphism.

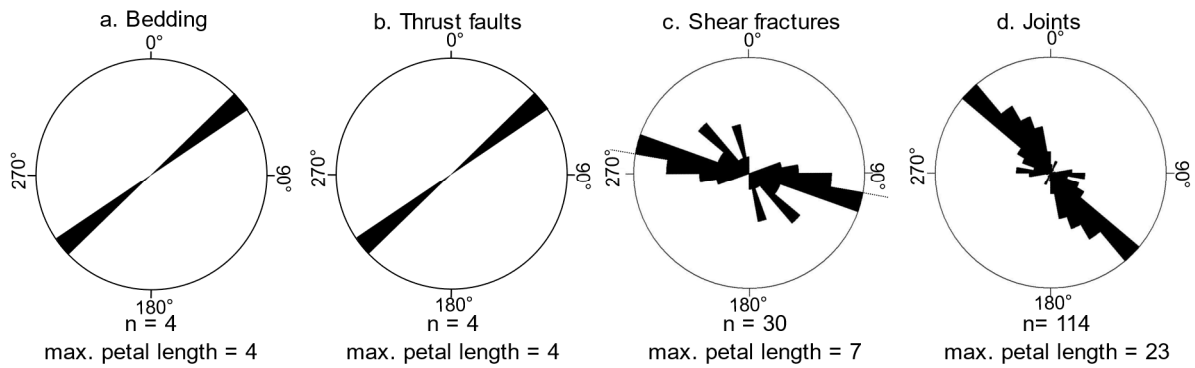


**Figure 3.** Orientations of different fluid flow controlling features. The tick marks on the perimeter of 3c show the trend of the largest fault in the field site ( $280^{\circ}$  to  $100^{\circ}$ ).

Sixty-nine sandstone band thicknesses were measured along a scanline perpendicular to the bands. Figure 4 shows a graphical representation of the sedimentary scanline. A digital caliper was used for their measurement and a histogram of the thicknesses is presented in figure 5. Almost all sandstone bands were under 1cm thick, but the thickest was significantly more at 7cm. Sandstone bands less than 1mm may be underestimated due to the difficulty of identifying such small features in the field. The distribution of sandstone band thicknesses is well described by a negative exponential distribution (figure 5). The sandstone bands represent a 3.6% net-to-gross of the total thickness of the red shale; similar ratios (2% sandstone) have been found in equivalent depositional environments (Basilici 1997).

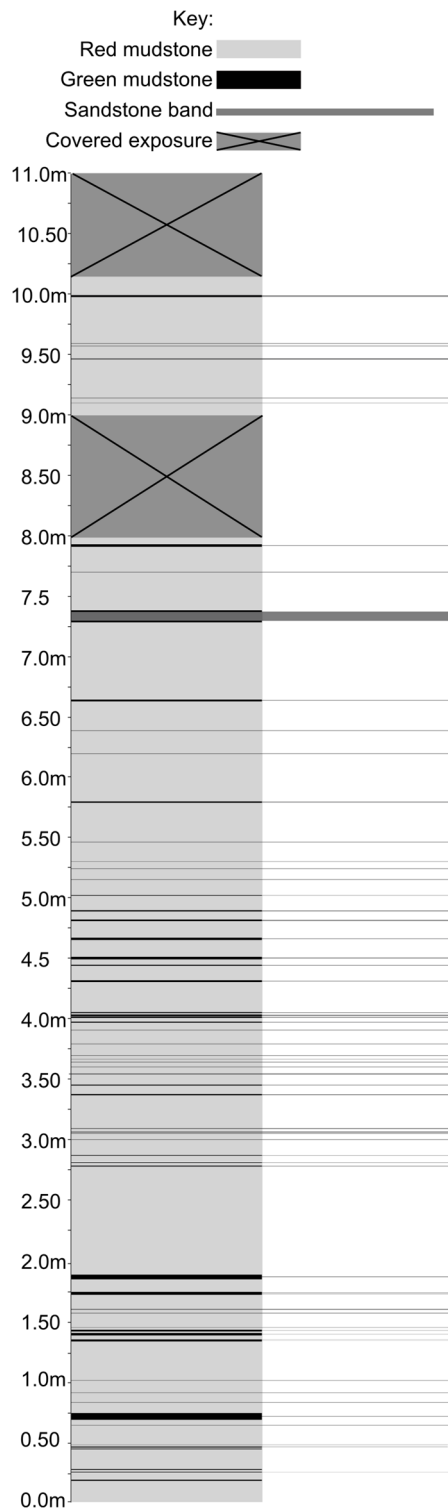


**Figure 4.** Sedimentary transect showing location and thickness of sandstone bands, including those with a surrounding green halo.

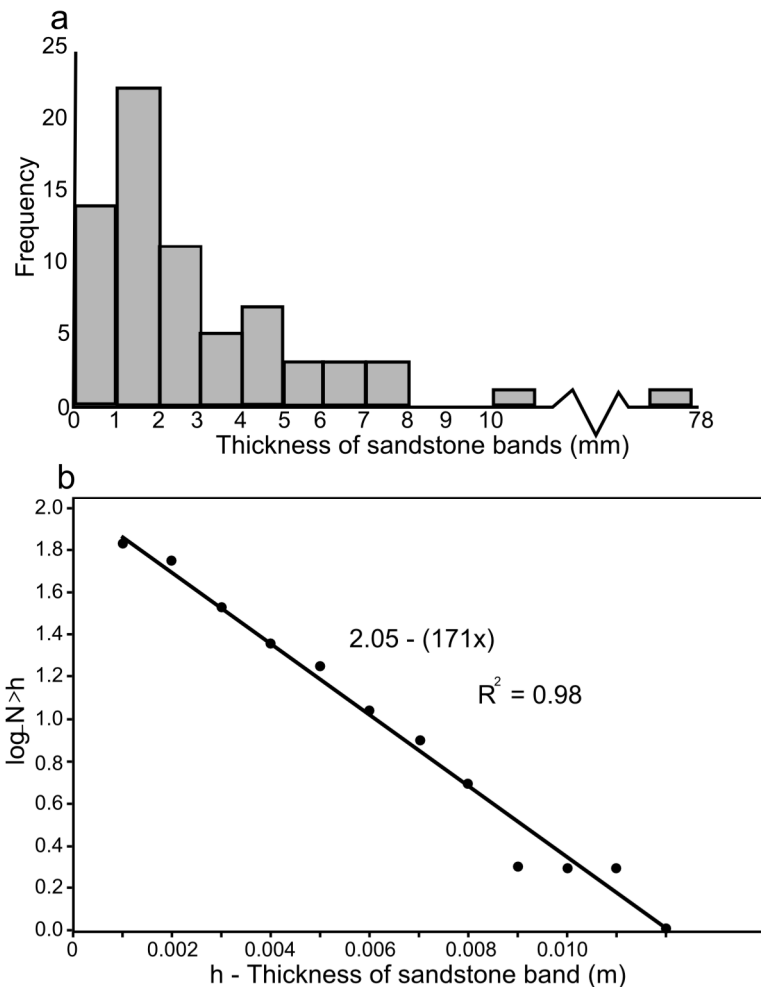


**Figure 5.** (a) Histogram of sandstone band thickness measured by digital caliper. (b) Cumulative frequency of sandstone bands of greater than thickness h ( $N>h$ ). Best fit line has  $R^2=0.98$ .

Thin sandstone sheets and isolated lenticular lobes are typical of outer fan areas of muddy submarine deposition systems (Basilici 1997). In other studies, similar looking structures have been classified as thin-bedded sand-mud couplets of Facies C2.3 in the deep water facies classification of Pickering et al. 1986. Some of the sandstone bands are continuous and can be traced along strike for tens of meters (>30 feet), whereas others occur as horizons of individual, distinct lenses which are likely caused by current ripples (Pickering et al. 1986). For the purposes of this study the bands are classified as high connectivity (continuous for greater than 1 meter, >3.3 feet), medium connectivity (continuous for between 10 cm and 1 m, >0.33 and <3.3 feet), and low connectivity (continuous for less than 10 cm, <0.33 feet). Although it should be noted that turbidites have been reported to have consistent connectivity for many miles (Plink-Blörklund and Steel 2004) significantly beyond the scale of this current study. Figure 6 shows how bands of these different connectivities tend to manifest in the field: even the low and medium connectivity bands can be laterally extensive and traceable for many tens of meters (>30 feet) despite the apparent internally unconnected nature of the lenses. Although the poor connectivity could be an artifact of the 2D slice presented by the outcrop, i.e. the isolated lenses of a low connectivity sandstone bands are a part of a connected unit in 3D, information presented later (figure 12) shows that the classification is a key determinant of the fluid flow behavior of the sandstone bands. Rarely, sandstone injectites sourced from the sandstone bands cut through the shale perpendicular to bedding. These injectites are thin (<2 cm,

<0.8 inches), they typically do not repeat within 50 m (160 feet) along strike of the bedding, and are only represented on the field study area in one location next to the main fault.



Figure 6. Schematic of the different levels of connectivity displayed by the sandstone bands. High connectivity bands are continuous for over 1m, medium connectivity bands have between 10cm and 1m long segments, and low connectivity bands are continuous.

### 2.3 Structural context

The rotation of the beds to their current near vertical dip, was likely due to folding accommodating NW-SE compression during the Caledonian Orogeny. The subsequent formation of the Whitehouse Shore Thrust Fault and several smaller synthetic thrusts is evidence of ongoing NW-SE compression (Ingham 1970). These faults strike sub-parallel to bedding and are exposed as bed-parallel gullies containing a thin (less than two cm) brecciated zone, which can be traced for tens of meters (>30 feet) across the exposure.

Conjugate dextral and sinistral strike-slip faults offset the beds and thrust faults. These have been interpreted as the final brittle deformation of the Caledonian Orogeny in the Late Silurian (Ingham 1978). The horizontal component of displacement on these strike-slip faults defined by offset of the subvertical bedding in the field site is usually less than 10m. This is a minimum value because the lack of slickenlines means that dip-slip displacement could not be determined.

The fault with the largest apparent displacement (labelled “main fault gully” in figure 2) was covered by coastal debris. A section of this fault exposed by seven volunteers with spades digging through coastal debris for a four hour tidal window, presented a fault core approximately 20 cm (0.66 feet) wide with loose, uncemented brecciated shale from which individual pieces can be removed by hand. A splay fault off the main fault shows a breccia varying from 1 to 5 cm wide bounded by slip surfaces. Both slip surfaces have sharp boundaries between the surrounding undeformed rock and the brecciated fault core. Sandstone bands are rotated clockwise into the fault, with some of this strain accommodated by shear fractures.

Shear fractures across the field site are orientated synthetic to the larger faults (figure 3c) and have horizontal offsets from several centimeters to a couple of millimeters, i.e. less than an inch. The shear fractures are primarily orientated WNW-ESE, synthetic to the main fault, with less common sets at NW-SE and NNW-SSE. Joints (fractures with no visible offset) are preferentially orientated to strike NW-SE (perpendicular to bedding) with some spread out to WNW-ESE and NNW-SSE (figure 3d).

### 3. Evidence for fluid flow

At the Whitehouse Shore there is clear evidence for two fluid flow episodes within the fractures and sandstone bands of the Myoch Formation red shale. The earliest fluid flow episode caused a phase of calcite cementation. The second fluid flow episode caused diagenesis of the red shale into green halos around fractures and sandstone bands.

Calcite cementation within this outcrop of the Myoch formation occurs in two forms: (1) as veins within fractures and (2) as pore-filling cement within sandstone bands (figure 7). Calcite veins can be up to 2 cm (0.79 inches) thick (figure 7a) but are predominantly 1-3 mm thick (figure 7c). The calcite

fills a subset of fractures; other adjacent fractures and fractures of similar orientations may contain no cement. In the thicker veins multiple stages of cementation are visible. Calcite was identified within the sandstone bands by the reaction with hydrochloric acid whereas the shale beds do not react.

Green halos surround a subset of the fractures and sandstone bands (figure 7). The halos typically extend less than one centimetre from fractures or bands and show a sharp contrast with the surrounding red shale. Green alteration in shale has previously been demonstrated to be due to the reduction of  $Fe^{3+}$  to  $Fe^{2+}$  (Mykura and Hampton 1984) along with transportation by diffusion of several minerals (Borradaile et al 1991). The red shale was likely deposited in oxidizing conditions, the overlying and underlying green shale layers are indicative of earlier and later reducing depositional conditions respectively. It is therefore likely that post-depositional fluid movement in the subsurface acted to reduce mineral oxides in the red shale. Regardless of the origin of the halos, this chemical alteration can be used to identify individual fractures that have acted as conduits for fluid flow (c.f Eichhubl et al. 2009).

Due to sampling restrictions, we were unable to sample the sandstone bands to determine which specific bands or parts of individual bands hosted calcite cement. However, where checked, these bands always reacted with HCl, indicating the presence of calcite. Therefore we have taken that those bands which were part of the second fluid flow episode creating the green halos also hosted the earlier calcite-precipitating flow episode.

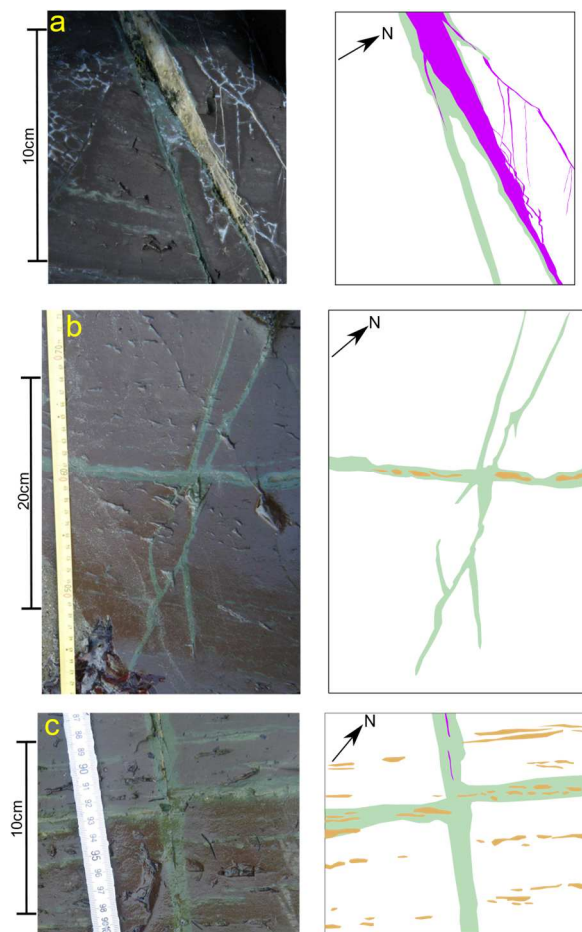


**Figure 7.** Examples of evidence for fluid flow where in the right hand digitisations: yellow represents sandstone bands, green the green halos, and fuchsia the calcite veins. (a) One of the thicker carbonate veins containing multiple stages of carbonate deposition. Green halos can be observed at

the lower side of the carbonate vein and on both sides of the unfilled fracture intersecting the vein. The palest white is due to salt efflorescence and is not related to tectonic veining. (b) Network of joints with surrounding green halo intersecting an example of a low connectivity sandstone band also surrounded by green halo. (c) Thin carbonate vein with surrounding green halo runs down the centre of the photograph. Vein sinistrally offsets low connectivity sandstone band with surrounding green halo. Ruler scales are in centimetres.

There is clear field evidence that calcite veins and cements preceded the formation of the green halos. Cross-cutting relationships showing green halo fractures terminating against calcite filled fractures (figure 8a) are repeated throughout the field site, whereas the converse was never observed. Additionally, in places the margin of calcite veins have acted as a focus for subsequent fracturing. Where this has occurred green halos are confined to only one side of the fracture (figure 8b). The calcite vein has acted as a barrier, stopping the fluid reacting with the opposite fracture wall.

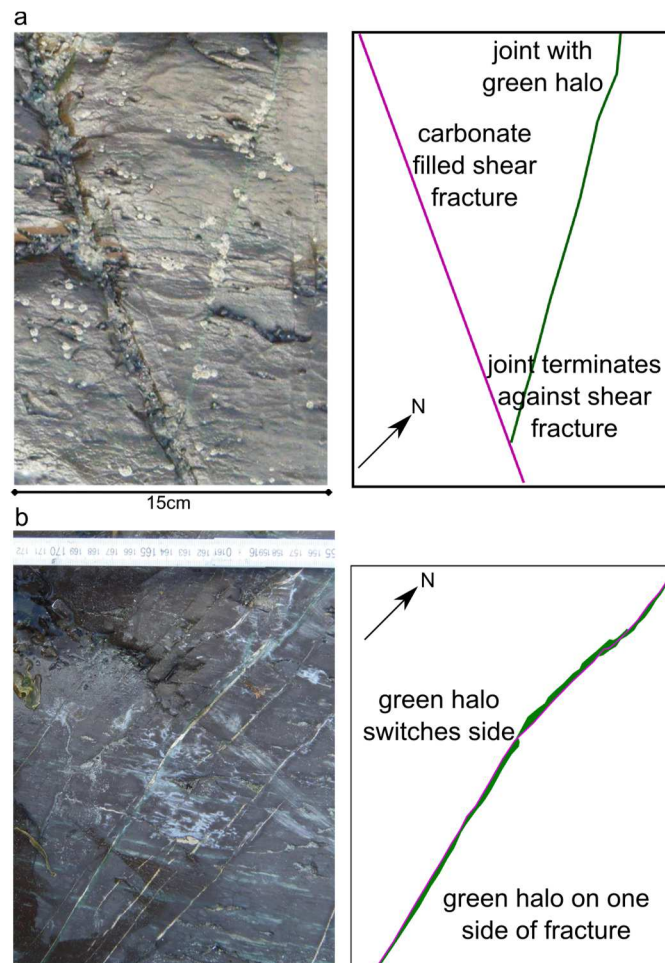


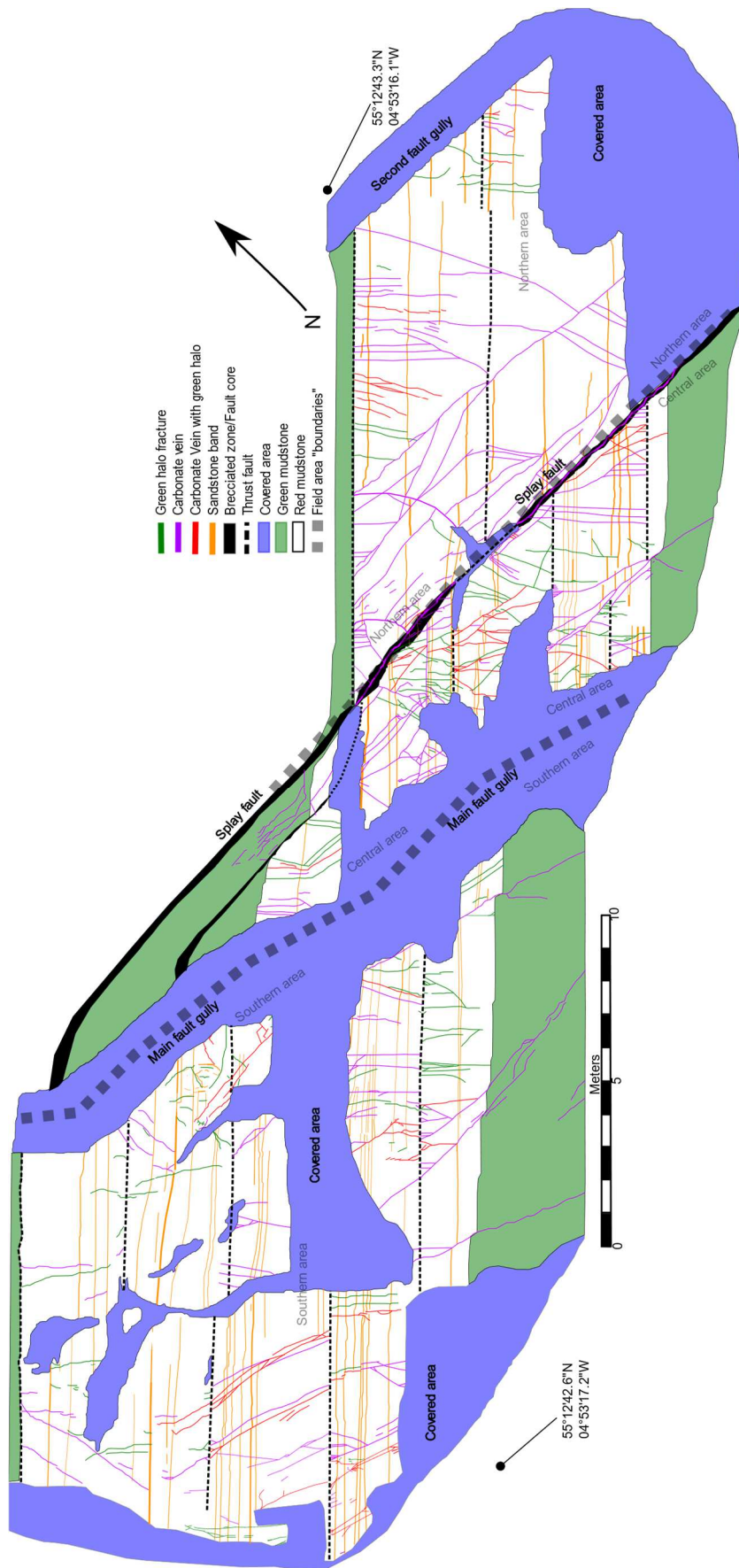
Figure 8. (a) Carbonate vein with shear movement. Joint with green halo terminates against pre-existing carbonate vein. (b) Green halo confined to one side of the fracture implying the carbonate in the vein acted as a barrier to chemical alteration on the other side. Where the green halo switches side there is a jog in the fracture and cracks in the carbonate so the reducing fluid may have transferred which side of the vein it was on at this point. In this and subsequent figures, schematics are used to illustrate the geometrical relationships because the details do not show up particularly clearly in photographs.

#### 4. Spatial distribution of features that may have facilitated fluid flow

Figure 9 shows a map of the fractures and sandstone bands as identified in the field. The map was established by defining a one-metre square string grid over the field site. Each square meter was photographed and interpretations annotated directly onto the photographs in the field during several low-tide “windows”. These were then digitised and stitched together to make an initial map. The map was then ground-truthed during subsequent low-tides to ensure that stitching the images had preserved the geometry, and to ensure that fine details were included with particular attention to the connections between the features. All fractures displayed calcite fill, green halos or both. Large sandstone bands all displayed green halos, small, unconnected bands that are too small to be included in the map sometimes had no halo.

The fracture density (defined as fracture mid-points per m<sup>2</sup>) of calcite filled and green halo fractures was counted using 46 circular scanlines; with diameters of 0.6 to 1.2 meters or 2 to 4 feet (Mauldon et al. 2001). Scanline diameter was selected to be larger than the blocks between fractures to ensure an adequate rate of sampling (Rohrbaugh et al. 2002), and due to unpredictable tidal debris cover, locations were selected to ensure adequate exposure within the scanline area.

**Figure 9.** Distribution of fractures sandstone bands and thrust faults colour coded by diagenetic evidence for fluid flow. Areas unobservable due to being covered by coastline debris are shown in blue and labelled as “covered area”. The thick dotted grey lines and text indicate how the field is split into the southern, central, and northern areas in subsequent figures.



Shear fractures have orientations synthetic or antithetic to the main faults, and joints generally bisect the conjugate shear fractures (figure 3). The calcite veins were often observed to be within the long, conjugate shear fractures. Conversely, green halos are more common around shorter NW-SE trending fractures, which tend to have no observable shear offset.

The field observations indicate that areas bounded by the main fault and splay fault have differing fracture properties. To aid discussion, the field area has been split up into “southern area” between South-West boundary and the Main Fault Gully, “central area” between the Main Fault Gully and the Splay Fault, and “northern area” between the Splay fault and the North-East boundary labelled on figure 10 as Second Fault Gully. Both the calcite veins and green halo fractures are highest density in the central area between the main fault and the splay fault (figure 10). The two particularly high-density values for calcite veins (labelled as “a” and “b” on figure 10) were caused by ladder geometry fractures between the splay fault and close proximity synthetic shear fractures. The calcite veins also show relatively high density in the northern area whereas the green halos do not, this distribution can clearly be seen in the detailed fracture map of figure 9 where very few green halos are located in the northern area.

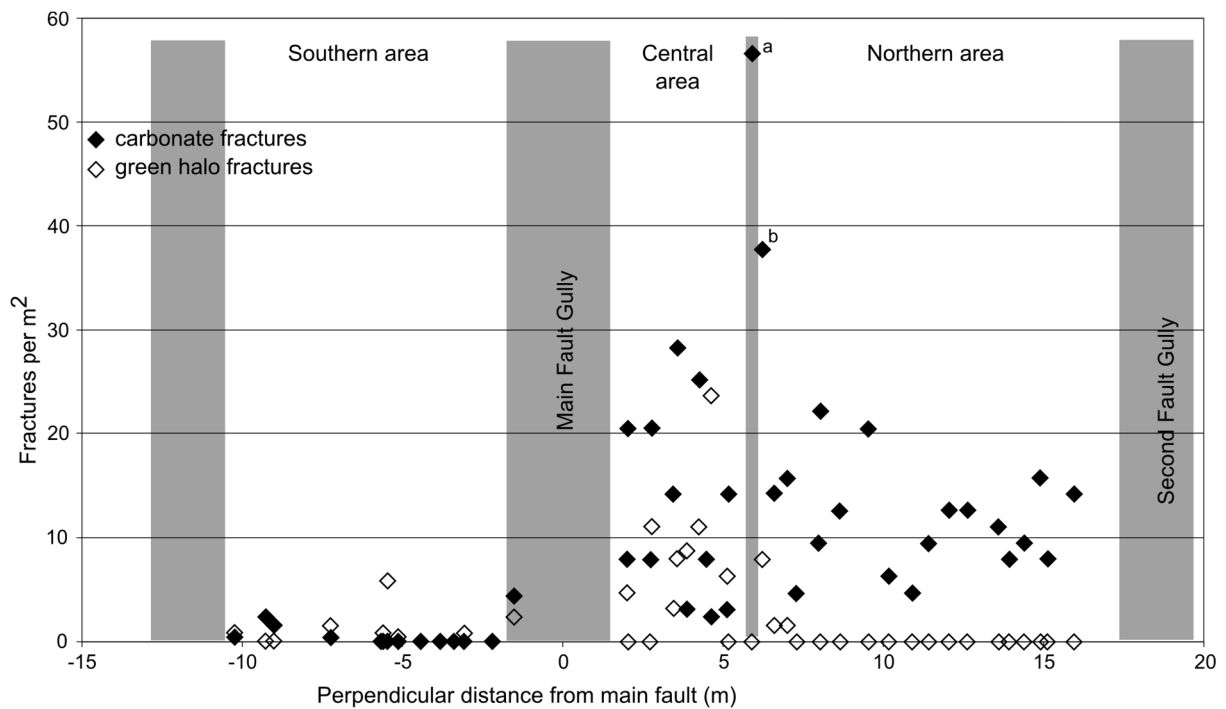


**Figure 10.** Fracture density across field site for carbonate veins (filled markers) and fractures with surrounding green halo (empty markers). Grey vertical bars show locations of “Main Fault Gully” and “Splay Fault” relative to where circular scanline data were collected. Locations of vertical bars correspond with the labelled faults and split the data into the southern, central, and northern areas as shown on figure 9. Each datum shows the value recorded from one circular scanline. The median values for carbonate fracture 8 density are 0.0, 14.1, and 11.8 for the southern, central, and northern area respectively; the median values for green halo fractures are 0.2, 7.1, and 0.0.

Orientation data were collected from 146 fractures within the detailed mapped area shown on figure 9. Figure 11 shows the orientations of the fractures divided into opening and shear mode (figure 11 b and c) and also by type of fluid alteration (figure 11, d, e, and f).

The sandstone bands are consistently steeply dipping (almost vertical) and strike SW-NE (figure 11 a). All fracture classifications (opening and shear mode and also both fluid flow alteration types) have strikes within 45° of NW-SE. However the orientations are not spread evenly within this area as some of the fracture types show particular clusters, highlighted on figure 11 (e.g. c1-c5 on Figure 11-c).

Joints and shear fractures have slightly different orientation distributions. The joint orientations are clustered around strikes of W-E (figure 11 c1 and c2), NW-SE (figure 11 c2 and c5) and also NNE-SSW (figure 11 c3). The shear fractures have much fewer orientation data than the joints, however the shear fractures appear to show a cluster striking N-S and also W-E (figure 11 b1 and b2 respectively). Although there are also some shear fractures striking NW-SE, there are proportionally less in this orientation than the joints.

The green halo fractures also show differences in orientation distribution to those fractures with calcite fill. A high proportion of the green halo fractures were clustered around NW-SE strikes (figure 11 d2 and d4), and a smaller proportion were clustered around E-W strikes (figure 11 d1 and d3). While the calcite filled fractures also have a small cluster around NW-SE strikes (figure 11 e2 and e4) there was a greater proportion clustered around E-W strikes (figure 11 e1 and e3). Additionally, the calcite filled fractures also show a small cluster around a strike of N-S. The fractures which hosted both fluid flow events cluster around E-W strikes (figure 11 f1 and f3) and NW-SE (figure 11 f2 and f4) and a smaller proportion striking N-S.

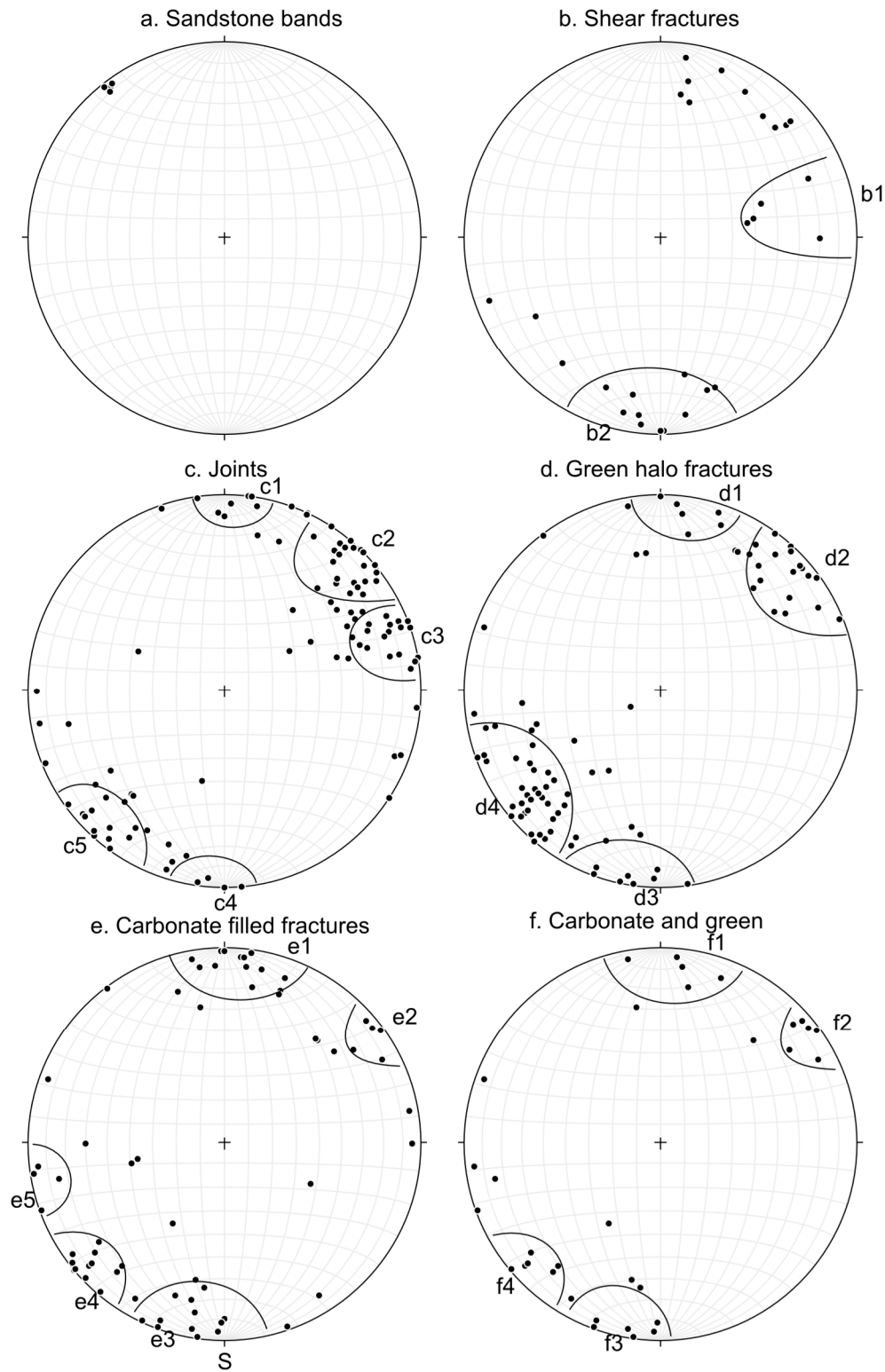


**Figure 11.** Orientations of different features. a. shows orientation data taken for four of the sandstone bands. b. and c. is fracture data split into shear fractures and joint. d. and e. show fracture orientation data grouped by the type of evidence for fluid flow. The orientations shown in “f, carbonate and green” is a combined subset from both “d, green halo fractures” and “e, carbonate filled fractures” and contains the fractures which appear in both fluid flow episodes. Stereonets were created using “Stereonet 9” (Allmendinger et al. 2011, Cardozo and Allmendinger 2013).

Field evidence for fluid flow demonstrates that the architecture and the length of each sandstone band controls its connectivity to the wider fluid flow network. The internal connectivity of the sandstone bands (figure 6) strongly correlates with the likelihood of a sandstone band having hosted fluid flow; high connectivity sandstone bands were far more likely to be surrounded by green halos than the low connectivity sandstone bands (figure 12). Five of the six (83%) high connectivity sandstone bands hosted fluid flow compared with only nine of the twenty seven (33%) low connectivity sandstone bands. The lateral extent of the sandstone bands (see figure 12 for definition) also plays a role with the longer bands being more likely to host fluid flow. Fourteen of the thirty three (42%) high extent sandstone bands hosted fluid flow compared with only one of the five (20%) low extent bands (figure 12). Although there is not as strong a relationship between the extent of the sandstone bands and their likelihood to have hosted diagenetic fluid flow as with connectivity, the observations are consistent with longer sandstone bands being more likely to intersect with other features that are open to fluid flow.

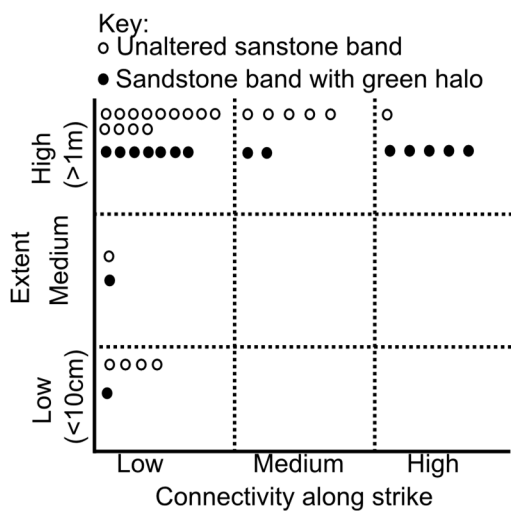


**Figure 12.** Comparison of the influence of connectivity (defined in figure 6) and extent on the likelihood of a sandstone band having a green halo. Lateral extent measures how far across the outcrop a sandstone band could be traced (even if that band was low connectivity and made of isolated lenses). Each dot shows a sandstone band classified by its observed connectivity and extent with the presence or absence of green halo. For example, out of the five of the sandstone bands with both low connectivity and low extent only one has a green halo, whereas five out of six do for sandstone bands with both high connectivity and high extent.

The sandstone bands are separated by irregular thicknesses of shale. If we assume that shale deposition is relatively constant, then the spacings between the sandstone bands may provide information about the timing of events which caused the turbidite flows depositing the coarser grained material. The spacing of the sandstone bands were measured to the nearest half centimetre using survey tape laid perpendicular to the bedding. The majority of the sandstone bands are spaced at intervals smaller than 0.1 m (0.33 feet) (figure 13a), although two intervals are much wider than the others at 0.66 m and 0.81 m (2.2 and 2.7 feet respectively). A negative exponential trend could be fit to the spacing distributions (figure 13 b), although the two widest spacings were not used in this fit due to not being sufficiently sampled to show a trend at these wider spacings.

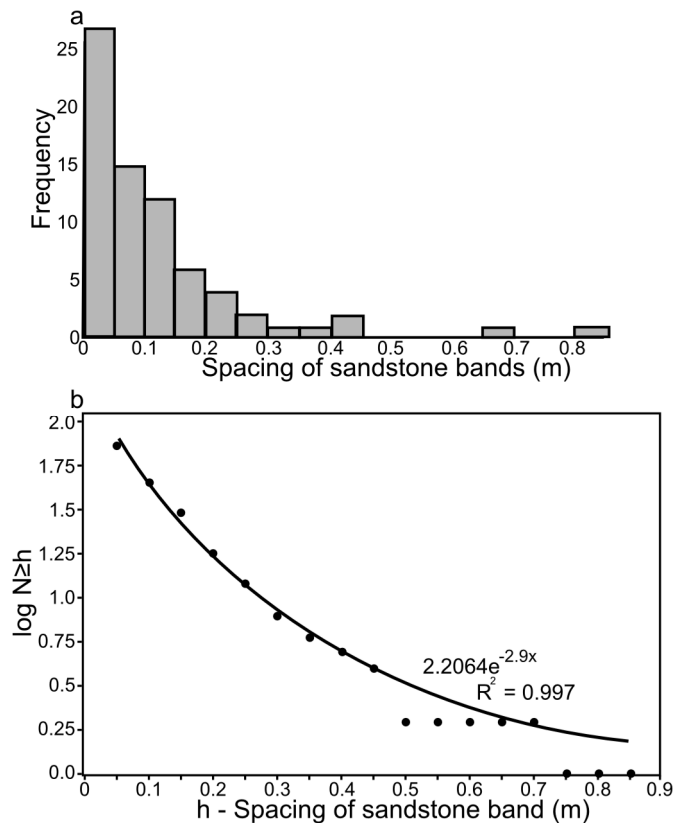


**Figure 13.** (a) histogram of spacing of the sandstone bands. (b) Cumulative frequency of spacing of sandstone bands of where spacing is h. An exponential is fitted to the data of 0.45m and under, as above this value then the sandstone bands are not sufficiently sampled, the best fit line shows an  $R^2=0.997$  and formula of  $y=2.2064e^{-2.9x}$ , for the data of 0.45m and under.

## 5. Connectivity of fluid flow features

Both calcite and green halos are restricted to within or very close to the highest permeability features in the rock, demonstrating that the fluids that caused these diagenetic effects were confined to networks comprising fractures, thrust faults, strike-slip faults and sandstone bands. The map in figure 9 was used to explore the network connectivity of these features and the differences between the two recorded fluid flow episodes. Connectivity was defined by counting how many connections each mapped fracture had with the other fractures, thrusts, and sandstone bands. The true 3D network may have more connectivity than the exposed 2D network, which was used to collect the connectivity data (Odling et al. 1999). However, the 2D network is the only viable way to collect field data on the connectivity between the features.

Figure 14 shows fracture connectivity for the three areas of the map, the southern, central and northern areas. When the fracture network is considered in isolation (i.e. not considering the sandstone bands or thrust faults) the majority of fractures have one or zero connections (figure 14a, b, c). For fluid flow to travel through such a potential fluid pathway then there must be at least two connections so as not to make a “dead end”. The first thing to note is that the fracture connectivity is lowest in the southern area, highest in the central area, and the northern area connectivity is approximately mid-way between the other two areas. This pattern of fracture connectivity correlates with the fracture density (figure 10). The higher fracture density of the central and north areas means that a higher proportion of fractures have two or more connections, compared with the southern area. However the central and northern area still have a median connectivity of 1, indicating that at least half of the fractures are still visible as “dead ends” in the exposed 2D fracture

network. Such low values of individual fracture connectivity might usually be indicative of fracture network with low hydraulic connectivity; however the calcite and green halos show that these fractures have been utilised as part of fluid flow episodes in the past.

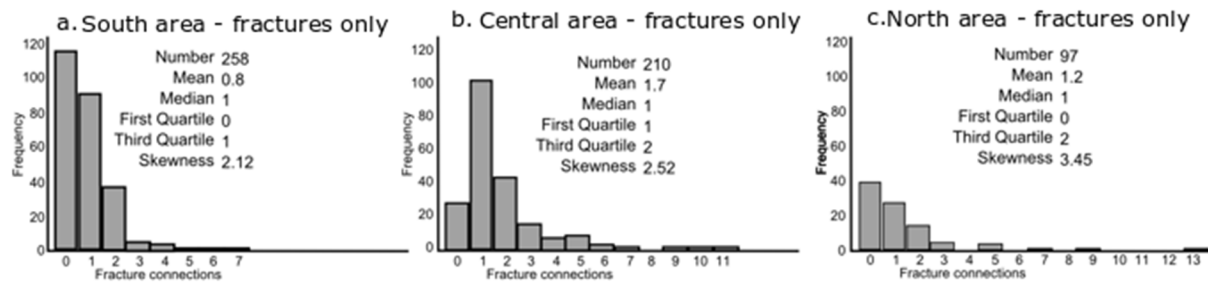


Figure 14. Histograms showing the frequency of fracture connectivity. The x-axis shows how many times each fracture intersects with another fracture. The data has been split between the three field areas shown in figure 8.

If there had not been any diagenesis to provide evidence that the sandstone bands were utilised during flow episodes, then it would have been standard practice to examine the fracture network connectivity alone. In figure 15 the connectivity of the combined flow network is calculated by including the sandstone bands and thrusts when counting the connections of each fracture. This means that some fractures which may have previously been considered isolated or dead-ends are now connected to the flow network by intersections with sandstone bands. The full fluid flow network (fractures and bands) for the earlier calcite-precipitating fluid flow episode (figure 14) has higher connectivity than when considering the fracture network alone. This enhanced connectivity is shown by the lower proportion of fractures with zero or one connection. A similar pattern is seen for the fractures and bands in the later “green halo” fluid flow episode (figure 14 b). This indicates that the sandstone bands are connecting otherwise isolated fractures. The full network has a median number of connections per fracture of 2 in each area (figure 15) compared to the fractures alone (figure 15). It is also worth noting that even in the southern area, where fracture density is low, the influence of the sandstone bands is enough to triple the upper quartile number of connections per fracture.

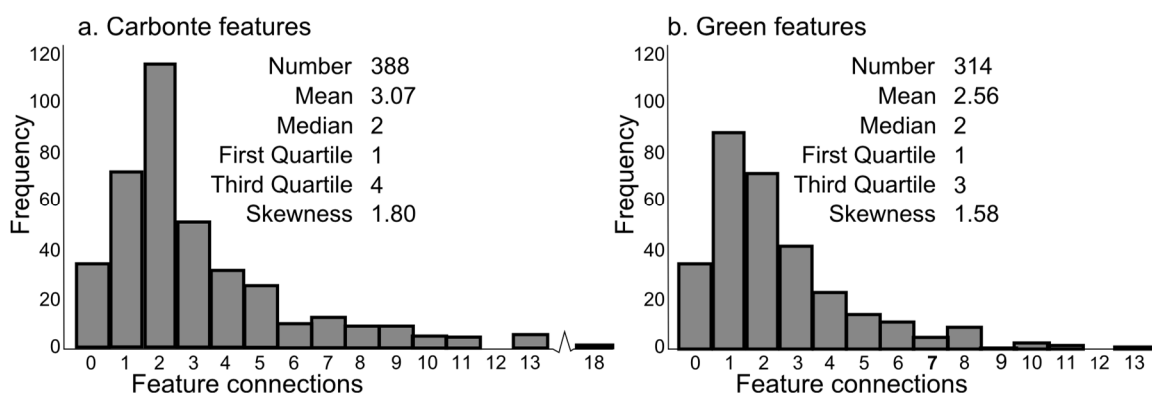


Figure 15. Histograms of connectivity of (a) carbonate filled fractures and (b) green halo fractures. Connectivity in this case includes when the fracture connects with all other features of that fluid flow episode, i.e. including connections with sandstone bands and thrust faults.

## 6. Discussion

### 6.1 How has the network connectivity influenced fluid flow through the shale over time?

The bulk permeability properties of the shale will have been strongly influenced by the connectivity of the permeable features during the geological history of the shale. An increase in average fracture connectivity, due to fracture initiation or propagation would increase the likelihood of complete fracture pathways forming which transverse the shale layer. Conversely, should a key network connection close then the unit could return to more sealing behaviour. In the field example presented in this paper, the main fault could be considered such a key connection. If the main fault were closed to fluid flow (for instance by diagenesis), but other pathways remained open, then the shale would not become a seal despite a likely significant drop in overall bulk permeability. Examining the differences between the two fluid flow networks captured in this outcrop provides valuable insights into the hydraulic history of this shale.

Initially after deposition and burial, the shale formation would have had very low porosity (Aplin and Macquaker 2011) and therefore low permeability (Yang and Aplin 2007, Armitage et al. 2011). Prior to any fracturing of the rock, there would have been no hydraulic connectivity between the sandstone bands except for via the rare sandstone injectites. The first deformation features are the folding and bedding-parallel thrust faults. The folding resulted in the exposed Whitehouse Formation having sub-vertical dip. No fold-related fracturing was recorded by Ingham (1978) or by this study so new connections between sandstone bands may not have formed at this stage. The thrust faults are related to the Whitehouse Shore Thrust Fault which dips to the north-west (figure 2). During this tectonic event, the thrust faults may have become critically stressed (Barton et al. 1995) and could have provided potential fluid flow pathways between any sandstone band that was intersected and offset.

The next stage of deformation was the formation of the sub-seismic scale strike-slip faults (Ingham 1978). These faults and related fractures are well orientated to intersect with many of the sandstone bands. These intersections, and the fact that the fractures tend to be relatively large features cutting through much of the shale, formed a well-connected network. This network was then exploited during the first fluid episode which left evidence of calcite precipitation. However this calcite precipitation, or other possible effects such as stress changes, subsequently acted to close many of these larger faults and fractures such that for the second fluid flow episode, which created the green halos, there were fewer large features contributing to the fluid flow network. This effect is particularly strong in the Northern Area of the field site, where the density of fractures contributing to the fluid flow network decreases dramatically between the two fluid flow episodes (figure 10); although some fractures did remain open during both fluid flow episodes (figure 15 b). Conversely, the central area maintained high fracture density between the fluid flow episodes, this may be due to the closely spaced main fault and splay fault (figure 9). Such fault interaction areas have previously been recorded as having enhanced fluid flow rates caused by high fracture density (Curewitz and Karson 1997, Gartrell et al. 2004, Ligtenberg 2005), including in some shale gas reservoirs (Gale et al. 2007).

The significant drop in the number of conductive fractures of the Northern Area in the time between the two fluid flow episodes would normally be expected to cause a decrease in connectivity (Harris et al. 2003, Berkowitz 2005); particularly when compared to the central area which did not experience a significant drop in fracture density. However, despite the closure of the longer fractures after the first calcite precipitating flow episode, flow network connectivity was maintained

because of the influence of the sandstone bands (figure 15) and the propagation of new fractures (figure 11 e). Although the flow network through the shale would now be more tortuous due to the interconnectivity required between the fractures and sandstone bands. Since the bands are perpendicular to the fractures, the result is a very well connected network for flow, and this unit did not behave as a seal. However, if only fractures had been considered, the density of open fractures would not have been enough to form connected networks through the shale, and the unit wrongly classified as sealing. These high permeability sandstones are small scale versions of the thief zones within seals or high permeability streaks observed in reservoir rocks (Felsenthal and Gangle 1975).

## 6.2 The distribution of the sandstone bands

Prediction of risks and opportunities remains the goal of much applied geoscience during hydrocarbon or geothermal exploration. The statistically constrained relationships (figures 5, 10, and 13) of the fluid-flow features indicate that such combined sedimentary-structural networks could be predictable.

Naturally, during any exploration a well-exposed outcrop will not be present, so it is important to ask how many of these features would have been picked up in wireline logs. From discussion with industry the limit of high resolution wireline logging is 5mm. Most of the sandstone bands are below this thickness and would therefore not be detected in an exploration setting; 82% of the sandstone bands with green halos had thicknesses below 5mm, whereas 78% of the bands with no halo (i.e. not connected to the network) had thicknesses below 5mm. There are no significant differences in ratio of number bands with green halos to those without, above or below this 5 mm threshold, indicating that thickness is not key factor for fluid flow. Given the key role that the sandstone bands have within the flow network, it would be desirable to be able to predict the thickness and spatial distribution of the bands with the greatest lateral extent, since these may be below detection threshold. Figure 5 showed that there is a relationship between the thicker and thinner bands in this study, but does this relationship hold for much thicker bands (e.g. >10cm)?

Studies of thicker turbidites (>10 cm thickness, >3.9 inches) in submarine fan depositional systems report thickness-frequency distributions that are exponential (Sinclair and Cowie 2003), log-normal (Talling 2001) or power law (Hiscott et al. 1992) and that these distributions may be site specific. A complicated range of factors affect thickness distributions, such as location within depositional setting and magnitude of triggering event (Carlson and Grotzinger 2001). The variations in thickness distribution have also been attributed to channelised vs nonchannelised material flows resulting from depositional topography (Carlson and Grotzinger 2001) and to buoyancy changes as the turbidity current “thins” during transport and deposition (Pritchard and Gladstone 2009). Log-normal distributions have been attributed to under-sampling of thin beds, although Talling (2001) disputed whether this is due to under-sampling or a true reflection of material deposition.

The data presented in this study, in combination with those of Sinclair and Cowie (2003) suggest that the distribution of turbidite thickness within an individual turbidite sequence is well modelled by an exponential distribution (figure 16). However, clearly, the parameter values that govern the exponential distribution vary. This is to be expected; for example, the statistics of turbidites triggered by floods are likely to vary between locations with differing climates, whereas the statistics of turbidites triggered by earthquakes will vary based on the earthquake magnitude-frequency distribution of proximal faults. Further, at a given site, turbidite thickness will decrease with increasing distance from the turbidite source (i.e. toward the edge of the fan). While a relatively small amount of studies have been conducted on the thickness of proximal and distal turbidites, even fewer have been published on turbidite thickness as a function of their lateral extent. To

predict sandstone band thickness and spacing distributions in a turbidite sequence, not only should more data be collected from multiple outcrops (ideally including exposures both parallel and perpendicular to bedding) but these data should be pooled to develop generalisable statistical models based on turbidite triggering mechanism and location within the turbidite fan.

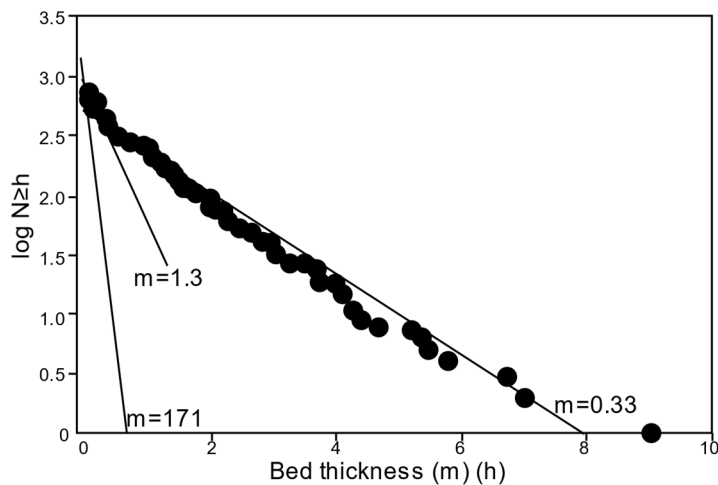


**Figure 16.** Cumulative frequency - thickness plot of turbidite thicknesses of the Annot Sandstone, data from Sinclair and Cowie (2013). A regression line with slope of 0.33 fits the data, for the smallest turbidites the slope of the regression line steepens to 1.3. The 171 sloping line is an approximation of the fit to the data presented from figure 5

### 6.3 Modelling approach for such small scale fluid flow networks.

Discrete fracture network (DFN) modelling would be a typical solution to further investigate such a sedimentary-structural flow network. It is beyond the scope of this current paper to produce a DFN model but the observations and data can inform how a DFN model could be constructed. This field study effectively presents a 2D window into the natural complicated 3D system, which would be modelled in a DFN. The observations made from the 2D outcrop, such as the central zone of high fracture connectivity surrounded by closely spaced faults, would be used to directly inform a modelled 3D network.

The sandstone bands would be added into the DFN as a 'fracture set'. The set up of this hypothetical DFN requires statistics that characterised the 'real' fracture and joint sets as well as an extra set that represent the sandstone band statistics. Data on such sandstone bands could be determined from image logs. Thinner band distribution is related to the seismic-scale beds (stats as discussed in paper) but attention paid to the source mechanism and basin topography (Sinclair and Cowie 2003), turbidite sources, such as fault movement (e.g. Goldfinger et al. 2007) or storm events (e.g. Malamud and Turcotte 2006, Gorsline et al. 2000). The joint frequency could be inferred from shale bed thickness and fracture frequencies, location and orientation of seismic scale faults (e.g Bonnet et al. 2001, Manzocchi et al. 2009).

These sedimentary and structural statistical distributions would then provide a basis to statistically populate a DFN style model, used to characterise bulk permeability properties of the unit. The field observations in this paper are a vital scale-bridge between core data (which does not give bulk rock properties) and seismic data (which cannot detect small but important network features) to inform how features in such networks interact to create fluid flow systems.

## 7. Conclusions

Mineral precipitation and diagenetic alteration has allowed tracing of pathways of palaeo-fluid flow episodes in the Myoch Formation at Girvan, Scotland. Such fluid flow is expected to be confined to the fracture networks within such low permeability rock. This study demonstrates that very thin (<1 cm) and relatively poorly connected sandstone layers can act to enhance the fracture connectivity. If these sandstone bands link otherwise isolated fractures, the bands would have played a crucial role in creating a connected network for fluid flow through the shale. The otherwise poorly connected fractures would not have been able to host such fluid flow without these sandstone bands. It is possible that such sedimentary structures in shales may be one route to forming sweet spots in shale gas reservoirs.

Sampling of such thin sandstone bands is confounded by their low thickness (below the resolution of wireline logging tools) and poor outcrop exposure, there is also a relative paucity of data on such thin layers. However the thin sandstone bands which are below the thickness of resolution show statistical distributions related to the thicker (>5mm) detectable bands in this study .

Although such fine-scale combined structural-sedimentary flow networks may seem too complex to realistically develop useful prediction methods, the observations in this paper suggest each of the important statistical properties of such fluid flow networks could be constrained, improving prediction of seal and fluid flow behaviour in similar settings.

## 8. References

- Allmendinger, R. W., N. Cardozo and D. M. Fisher (2011). Structural Geology Algorithms: Vectors and Tensors, Cambridge University Press.
- Aplin, A. C. and J. H. Macquaker. 2011, Mudstone diversity: Origin and implications for source, seal, and reservoir properties in petroleum systems, AAPG bulletin, v. 95, p. 2031-2059.
- Aplin, A.C., Fleet, A.J. and Macquaker, J.H., 1999. Muds and mudstones: Physical and fluid-flow properties: Geological Society of London, Special Publications, v. 158, p.1-8, doi:[10.1016/s0278-4343\(00\)00098-4](https://doi.org/10.1016/s0278-4343(00)00098-4).
- Armitage, P., D. Faulkner, R. Worden, A. Aplin, A. Butcher and J. Iliffe, 2011, Experimental measurement of, and controls on, permeability and permeability anisotropy of caprocks from the CO2 storage project at the Krechba Field, Algeria: Journal of Geophysical Research: Solid Earth, v. 116, p. 1978-2012, doi:[10.1029/2011jb008385](https://doi.org/10.1029/2011jb008385)
- Barton, C.A., Zoback, M.D. and Moos, D., 1995. Fluid flow along potentially active faults in crystalline rock. *Geology*, 23, pp.683-686, doi: 10.1130/0091-7613(1995)023
- Basilici, G., 1997, Sedimentary facies in an extensional and deep-lacustrine depositional system: the Pliocene Tiberino Basin, Central Italy: *Sedimentary Geology*, v. 109, p. 73-94, doi: [10.1016/s0037-0738\(96\)00056-5](https://doi.org/10.1016/s0037-0738(96)00056-5).
- Berkowitz, B., 1995, Analysis of fracture network connectivity using percolation theory: *Mathematical Geology*, v. 27, p. 467-483, doi:[10.1007/bf02084422](https://doi.org/10.1007/bf02084422).
- Bolton, A.J., A. J. Maltman, and Q. and Fisher, 2000, Anisotropic permeability and bimodal pore-size distributions of fine-grained marine sediments: *Marine and Petroleum Geology*, v. 17, p.657-672, doi:[10.1016/s0264-8172\(00\)00019-2](https://doi.org/10.1016/s0264-8172(00)00019-2)

- Bonnet, E., O. Bour, N.E. Odling, P. Davy, I. Main, P. Cowie, and B. Berkowitz, 2001, Scaling of fracture systems in geological media: *Reviews of geophysics*, v. 39, p. 347-383, doi:[10.1029/1999rg000074](https://doi.org/10.1029/1999rg000074).
- Borradaile, G.J., A. MacKenzie, E. and Jensen, 1991, A study of colour changes in purple-green slate by petrological and rock-magnetic methods: *Tectonophysics*, v. 200, p.157-172, doi: [10.1016/0040-1951\(91\)90012-h](https://doi.org/10.1016/0040-1951(91)90012-h).
- Bouma, A.H., P. H. Kuenen, F. P. and Shepard, 1962, *Sedimentology of some flysch deposits: a graphic approach to facies interpretation*: v. 168, Amsterdam: Elsevier.
- Burnside, N.M., Z. K. Shipton, B. Dockrill, and R. M. Ellam, 2013, Man-made versus natural CO<sub>2</sub> leakage: A 400 ky history of an analogue for engineered geological storage of CO<sub>2</sub>: *Geology*, v. 41, p.471-474, doi:[10.1130/g33738.1](https://doi.org/10.1130/g33738.1).
- Cardozo, N., and R. W. Allmendinger, 2013, Spherical projections with OSXStereonet: *Computers & Geosciences*, v. 51, p. 193-205. doi:[10.1016/j.cageo.2012.07.021](https://doi.org/10.1016/j.cageo.2012.07.021).
- Carlson, J. and J. Grotzinger, 2001, Submarine fan environment inferred from turbidite thickness distributions: *Sedimentology*, v. 48, p. 1331-1351, doi:[10.1046/j.1365-3091.2001.00426.x](https://doi.org/10.1046/j.1365-3091.2001.00426.x).
- Cartwright, J., M. Huuse, and A. Aplin, 2007, Seal bypass systems: *AAPG bulletin*, v. 91, p. 1141-1166.
- Curewitz, D., and J. A. Karson, 1997, Structural settings of hydrothermal outflow: Fracture permeability maintained by fault propagation and interaction: *Journal of Volcanology and Geothermal Research*, v. 79, p. 149-168. doi:[10.1016/s0377-0273\(97\)00027-9](https://doi.org/10.1016/s0377-0273(97)00027-9).
- Crimes, T.P., 1973, From limestones to distal turbidites: a facies and trace fossil analysis in the Zumaya flysch (Paleocene—Eocene), North Spain: *Sedimentology*, v. 20, p.105-131, doi:[10.1111/j.1365-3091.1973.tb01609.x](https://doi.org/10.1111/j.1365-3091.1973.tb01609.x).
- Davatzes, N.C., and A. Aydin, 2003, Overprinting faulting mechanisms in high porosity sandstones of SE Utah: *Journal of Structural Geology*, v. 25, p. 1795-1813, doi:[10.1016/s0191-8141\(03\)00043-9](https://doi.org/10.1016/s0191-8141(03)00043-9).
- Dewhurst, D. N., and A. F. Siggins, 2006, Impact of fabric, microcracks and stress field on shale anisotropy: *Geophysical Journal International*, v. 165, p.135-148, doi:[10.1111/j.1365-246x.2006.02834.x](https://doi.org/10.1111/j.1365-246x.2006.02834.x).
- Dockrill, B., and Z. K. Shipton, 2010, Structural controls on leakage from a natural CO<sub>2</sub> geologic storage site: Central Utah, USA: *Journal of Structural Geology*, v. 32, p. 1768-1782, doi:[10.1016/j.jsg.2010.01.007](https://doi.org/10.1016/j.jsg.2010.01.007).
- Eichhubl, P., P. S. D'Onfro, A. Aydin, J. Waters, and D. K. McCarty, 2005, Structure, petrophysics, and diagenesis of shale entrained along a normal fault at Black Diamond Mines, California—Implications for fault seal: *AAPG bulletin*, v. 89, p.1113-1137, doi:[10.1306/04220504099](https://doi.org/10.1306/04220504099).
- Eichhubl, P., N. C. Davatzes, and S. P. Becker, 2009, Structural and diagenetic control of fluid migration and cementation along the Moab fault, Utah: *AAPG bulletin*, v. 93, p. 653-681, doi:[10.1306/02180908080](https://doi.org/10.1306/02180908080).
- Evans, M.A., 1994. Joints and decollement zones in Middle Devonian shales: Evidence for multiple deformation events in the central Appalachian Plateau: *Geological Society of America Bulletin*, v. 106, p. 447-460, doi: [10.1130/0016-7606\(1994\)106<0447:jadczi>2.3.co;2](https://doi.org/10.1130/0016-7606(1994)106<0447:jadczi>2.3.co;2)

- Fairley, J. P., J. J. and Hinds, 2004, Rapid transport pathways for geothermal fluids in an active Great Basin fault zone: *Geology*, v. 32, p. 825-828, doi:[10.1130/g20617.1](https://doi.org/10.1130/g20617.1).
- Felsenthal, M., and F. J. Gangle, 1975, A Case Study of Thief Zones in a California Waterflood: *Journal of Petroleum Technology*, v. 27, p. 1385-1391, doi:[10.2118/5363-pa](https://doi.org/10.2118/5363-pa).
- Gale, J.F., S. E. Laubach, J. E. Olson, P. Eichhubl, and A. Fall, 2014, Natural fractures in shale: A review and new observations: *AAPG bulletin*, v. 98, p. 2165-2216, doi:[10.1306/08121413151](https://doi.org/10.1306/08121413151).
- Gale, J.F., R. M. Reed, and J. Holder, 2007, Natural fractures in the Barnett Shale and their importance for hydraulic fracture treatments: *AAPG bulletin*, v. 91, p. 603-622, doi:[10.1306/11010606061](https://doi.org/10.1306/11010606061).
- Gartrell, A., Y. Zhang, M. Lisk and D. Dewhurst, 2004, Fault intersections as critical hydrocarbon leakage zones: integrated field study and numerical modelling of an example from the Timor Sea, Australia: *Marine and Petroleum Geology*, v. 21, p. 1165-1179, doi:[10.1016/j.marpetgeo.2004.08.001](https://doi.org/10.1016/j.marpetgeo.2004.08.001).
- Gaus, I., 2010, Role and impact of CO<sub>2</sub>-rock interactions during CO<sub>2</sub> storage in sedimentary rocks: *International journal of greenhouse gas control*, v. 4, p. 73-89, doi:[10.1016/j.ijggc.2009.09.015](https://doi.org/10.1016/j.ijggc.2009.09.015).
- Glaser, K. S., C. K. Miller, G. M. Johnson, B. Toelle, R. L. Kleinberg, P. Miller, and W. D. Pennington, 2013, Seeking the sweet spot: reservoir and completion quality in organic shales. *Oilfield Review*, v. 25, p.16-29, doi:[10.3997/2214-4609.20143899](https://doi.org/10.3997/2214-4609.20143899).
- Goldfinger, C., A. E. Morey, C. H. Nelson, J. Gutiérrez-Pastor, J. E. Johnson, E. Karabanov, J. Chaytor, A. Eriksson, and S. S. Party, 2007, Rupture lengths and temporal history of significant earthquakes on the offshore and north coast segments of the Northern San Andreas Fault based on turbidite stratigraphy: *Earth and Planetary Science Letters*, v. 254, p. 9-27. doi:[10.1016/j.epsl.2006.11.017](https://doi.org/10.1016/j.epsl.2006.11.017).
- Gorsline, D.S., T. De Diego, and E. H. Nava-Sanchez, 2000, Seismically triggered turbidites in small margin basins: Alfonso Basin, western Gulf of California and Santa Monica Basin, California borderland: *Sedimentary Geology*, v. 135, p. 21-35, doi:[10.1016/s0037-0738\(00\)00060-9](https://doi.org/10.1016/s0037-0738(00)00060-9).
- Haney, M. M., R. Snieder, J. Sheiman, and S. Losh, 2005, A fault caught in the act of burping: *CWP Scientific Report*. v. 513. p. 219-223.
- Harris, S., E. McAllister, R. Knipe and N. Odling, 2003, Predicting the three-dimensional population characteristics of fault zones: a study using stochastic models: *Journal of Structural Geology*, v. 25, p. 1281-1299, doi:[10.1016/s0191-8141\(02\)00158-x](https://doi.org/10.1016/s0191-8141(02)00158-x).
- Hubert, J.F., 1966, Sedimentary history of upper Ordovician geosynclinal rocks, Girvan, Scotland. *Journal of Sedimentary Research*, v. 36, p. 677-699, doi:[10.1306/74d71541-2b21-11d7-8648000102c1865d](https://doi.org/10.1306/74d71541-2b21-11d7-8648000102c1865d).
- Ince, D., 1984, Sedimentation and tectonism in the Middle Ordovician of the Girvan district, SW Scotland: *Transactions of the Royal Society of Edinburgh: Earth Sciences*, v. 75, p. 225-237, doi:[10.1017/s0263593300013869](https://doi.org/10.1017/s0263593300013869).
- Ingham, J., 1978, Geology of a continental margin 2: middle and late Ordovician transgression, Girvan: *Crustal evolution in northwestern Britain and adjacent regions*, v. 10, p. 163-167.

- Kampman, N., N. M. Burnside, Z. K. Shipton, H. J. Chapman, J. A. Nicholl, R. M. Ellam, and M. J. Bickle, 2012, Pulses of carbon dioxide emissions from intracrustal faults following climatic warming: *Nature Geoscience*, v. 5, p. 352-358, doi:[10.1038/ngeo1451](https://doi.org/10.1038/ngeo1451).
- Kim, J. S., S. K. Kwon, M. Sanchez, and G. C. Cho, 2011, Geological storage of high level nuclear waste. *KSCE Journal of Civil Engineering*, v. 15, p.721-737.
- Lash, G.G. and T. Engelder, 2009, Tracking the burial and tectonic history of Devonian shale of the Appalachian Basin by analysis of joint intersection style: *Geological Society of America Bulletin*, v. 121, p. 265-277. doi:[10.1130/b26287.1](https://doi.org/10.1130/b26287.1).
- Lawson, J. D. and D. S. Weedon, 1992, *Geological excursions around Glasgow & Girvan*: Glasgow, Geological Society of Glasgow.
- Lehner, F.K. and W. F. Pilaar, 1997, The emplacement of clay smears in synsedimentary normal faults: inferences from field observations near Frechen, Germany: *Norwegian Petroleum Society Special Publications*, v. 7, p. 39-50, doi:[10.1016/s0928-8937\(97\)80005-7](https://doi.org/10.1016/s0928-8937(97)80005-7).
- Ligtenberg, J., 2005, Detection of fluid migration pathways in seismic data: implications for fault seal analysis: *Basin Research*, v. 17, p. 141-153, doi:[10.1111/j.1365-2117.2005.00258.x](https://doi.org/10.1111/j.1365-2117.2005.00258.x).
- Malamud, B. D., and D. L. Turcotte, 2006, The applicability of power-law frequency statistics to floods: *Journal of Hydrology*, v. 322, p. 168-180, doi:[10.1016/j.jhydrol.2005.02.032](https://doi.org/10.1016/j.jhydrol.2005.02.032).
- Manzocchi, T., J. J. Walsh, and W. R. Bailey, 2009, Population scaling biases in map samples of power-law fault systems: *Journal of Structural Geology*, v. 31, p. 1612-1626, doi:[10.1016/j.jsg.2009.06.004](https://doi.org/10.1016/j.jsg.2009.06.004).
- Mauldon, M., W. Dunne and M. Rohrbaugh Jr., 2001, Circular scanlines and circular windows: new tools for characterizing the geometry of fracture traces: *Journal of Structural Geology*, v. 23, p. 247-258, doi:[10.1016/s0191-8141\(00\)00094-8](https://doi.org/10.1016/s0191-8141(00)00094-8).
- Mykura, H., and B. P. Hampton, 1984, On the mechanism of formation of reduction spots in the Carboniferous/Permian red beds of Warwickshire: *Geological Magazine*, v. 121, p.71-74, doi:[10.1017/s0016756800027965](https://doi.org/10.1017/s0016756800027965).
- Odling, N.E., P. Gillespie, B. Bourguine, C. Castaing, J. P. Chiles, N. P. Christensen, E. Fillion, A. Genter, C. Olsen, L. Thrane, and R. Trice, 1999, Variations in fracture system geometry and their implications for fluid flow in fractured hydrocarbon reservoirs: *Petroleum Geoscience*, v. 5, p. 373-384, doi:[10.1144/petgeo.5.4.373](https://doi.org/10.1144/petgeo.5.4.373).
- Pickering, K., D. Stow, M. Watson and R. Hiscott, 1986, Deep-water facies, processes and models: a review and classification scheme for modern and ancient sediments: *Earth-Science Reviews*, v. 23, p. 75-174, doi:[10.1016/0012-8252\(86\)90001-2](https://doi.org/10.1016/0012-8252(86)90001-2).
- Plink-Björklund, P. and Steel, R.J., 2004. Initiation of turbidity currents: outcrop evidence for Eocene hyperpycnal flow turbidites. *Sedimentary Geology*, 165(1), pp.29-52.
- Pritchard, D. and C. Gladstone, 2009, Reversing buoyancy in turbidity currents: developing a hypothesis for flow transformation and for deposit facies and architecture: *Marine and Petroleum geology*, v. 26, p. 1997-2010, doi:[10.1016/j.marpetgeo.2009.02.010](https://doi.org/10.1016/j.marpetgeo.2009.02.010).

- Rohrbaugh Jr, M., W. Dunne and M. Mauldon, 2002, Estimating fracture trace intensity, density, and mean length using circular scan lines and windows: AAPG bulletin, v. 86, p. 2089-2104, doi:[10.1306/61eede0e-173e-11d7-8645000102c1865d](https://doi.org/10.1306/61eede0e-173e-11d7-8645000102c1865d).
- Sinclair, H. and P. Cowie, 2003, Basin-Floor Topography and the Scaling of Turbidites: The Journal of geology, v. 111, p. 277-299, doi:[10.1086/373969](https://doi.org/10.1086/373969).
- Talling, P. J., 2001, On the frequency distribution of turbidite thickness: Sedimentology, v. 48, p. 1297-1329, doi:[10.1046/j.1365-3091.2001.00423.x](https://doi.org/10.1046/j.1365-3091.2001.00423.x).
- Terzaghi, R. D., 1965, Sources of error in joint surveys: Geotechnique, v. 15, p. 287-304, doi:[10.1680/geot.1965.15.3.287](https://doi.org/10.1680/geot.1965.15.3.287).
- Yang, Y. and A. C. Aplin, 2007, Permeability and petrophysical properties of 30 natural mudstones: Journal of Geophysical Research: Solid Earth, v. 112, p. 1978–2012, doi:[10.1029/2005jb004243](https://doi.org/10.1029/2005jb004243).
- Walker, R.G., 1978, Deep-water sandstone facies and ancient submarine fans: models for exploration for stratigraphic traps: AAPG Bulletin, v, 62, p. 932-966, doi:[10.1306/c1ea4f77-16c9-11d7-8645000102c1865d](https://doi.org/10.1306/c1ea4f77-16c9-11d7-8645000102c1865d).
- Willmot Noller, N. and Daly, S., 2014, The contribution of heat production studies to geothermal exploration in Ireland: In EGU General Assembly Conference Abstracts, v. 16, p. 14114.
- Yielding, G., B. Freeman, and D. T. Needham, 1997. Quantitative fault seal prediction. AAPG bulletin, v. 81, p. 897-917, doi:[10.1306/522b498d-1727-11d7-8645000102c1865d](https://doi.org/10.1306/522b498d-1727-11d7-8645000102c1865d).
- Zhao, C., B. E. Hobbs, A. Ord, P. Hornby, S. Peng, and L. Liu, 2007, Mineral precipitation associated with vertical fault zones: the interaction of solute advection, diffusion and chemical kinetics: Geofluids, v. 7, p.3-18, doi:[10.1111/j.1468-8123.2006.00156.x](https://doi.org/10.1111/j.1468-8123.2006.00156.x).